

MEASURING THE STANDARD MODEL AND SEARCHING FOR
NEW PHYSICS WITH JET SUBSTRUCTURE USING THE ATLAS DETECTOR

A DISSERTATION
SUBMITTED TO THE DEPARTMENT OF PHYSICS
AND THE COMMITTEE ON GRADUATE STUDIES
OF STANFORD UNIVERSITY
IN PARTIAL FULFILLMENT OF THE REQUIREMENTS
FOR THE DEGREE OF
DOCTOR OF PHILOSOPHY

Maximilian Swiatlowski
March 2015

© Copyright by Maximilian Swiatlowski 2015
All Rights Reserved

I certify that I have read this dissertation and that, in my opinion, it is fully adequate in scope and quality as a dissertation for the degree of Doctor of Philosophy.

(Ariel Schwartzman) Principal Adviser

I certify that I have read this dissertation and that, in my opinion, it is fully adequate in scope and quality as a dissertation for the degree of Doctor of Philosophy.

(Su Dong)

I certify that I have read this dissertation and that, in my opinion, it is fully adequate in scope and quality as a dissertation for the degree of Doctor of Philosophy.

(Jay G. Wacker)

I certify that I have read this dissertation and that, in my opinion, it is fully adequate in scope and quality as a dissertation for the degree of Doctor of Philosophy.

(Blas Cabrera (??))

I certify that I have read this dissertation and that, in my opinion, it is fully adequate in scope and quality as a dissertation for the degree of Doctor of Philosophy.

(???)

Approved for the Stanford University Committee on Graduate Studies

Preface

This thesis tells you all you need to know about...

Acknowledgments

I would like to thank...

Contents

| | |
|--|----|
| Preface | v |
| Acknowledgments | vi |
| 1 Introduction | 1 |
| 2 The Standard Model, and the Theory of Strong Interactions | 2 |
| 2.1 Overview | 2 |
| 2.2 Spontaneous Symmetry Breaking, the Electroweak Force, and the Origin of Mass | 2 |
| 2.3 Quantum Chromodynamics and Strong Interactions | 2 |
| 3 Jets and Substructure | 3 |
| 3.1 The Goal of Jets, and Jet Algorithms | 3 |
| 3.2 Jet Substructure: Going Deeper | 3 |
| 3.3 Calculations with Jets | 3 |
| 4 Supersymmetry, <i>R</i>-Parity, and Naturalness | 4 |
| 4.1 The Problem of the Standard Model | 4 |
| 4.2 Supersymmetry: The Solution? | 4 |
| 4.3 <i>R</i> -Parity, and How to Violate It | 4 |
| 4.4 Naturalness, or the Pursuit of Beauty | 4 |
| 5 The Large Hadron Collider | 5 |
| 5.1 History | 5 |
| 5.2 Machine Design | 10 |
| 5.3 Luminosity, and Pileup | 10 |
| 5.4 Operations in 2010-2012 | 10 |
| 6 The ATLAS Detector | 11 |
| 6.1 History | 14 |

| | | |
|----------|--|-----------|
| 6.1 | Detector Components | 15 |
| 6.2 | Magnet Systems | 16 |
| 6.2.1 | Solenoid | 16 |
| 6.2.2 | Toroids | 16 |
| 6.3 | Inner Detector | 16 |
| 6.3.1 | Silicon Pixel Detector | 18 |
| 6.3.2 | Silicon Strip Tracker | 21 |
| 6.3.3 | Transition Radiation Tracker | 21 |
| 6.4 | Calorimeters | 23 |
| 6.4.1 | Electromagnetic Calorimeter | 23 |
| 6.4.2 | Hadron Calorimeter | 23 |
| 6.5 | Muon Spectrometer | 23 |
| 6.6 | Triggering | 23 |
| 6.7 | Data Quality | 23 |
| 7 | Jet Reconstruction with ATLAS | 27 |
| 7.1 | Clusters, Towers, and Tracks, Oh My | 27 |
| 7.1.1 | Cluster Calibration | 27 |
| 7.2 | Jet Calibration | 27 |
| 7.3 | Quark/Gluon Discrimination | 27 |
| 7.3.1 | Lots of subsections | 27 |
| 8 | Seeing Color at the LHC | 28 |
| 8.1 | Motivation | 28 |
| 8.2 | Reconstructing Color | 28 |
| 8.2.1 | Finding Top Quarks | 28 |
| 8.2.2 | Origin Corrections | 28 |
| 8.2.3 | Resolution Effects | 28 |
| 8.2.4 | Track and Cluster Uncertainties | 28 |
| 8.3 | Measuring Color | 28 |
| 8.3.1 | Unfolding | 28 |
| 8.3.2 | Results | 28 |
| 8.3.3 | Future Prospects | 28 |
| 9 | Searching for Supersymmetry with Super Jets | 29 |
| 9.1 | Motivation | 29 |
| 9.2 | Why Jet Substructure? | 29 |
| 9.2.1 | Total Jet Mass, and Other Variables | 29 |
| 9.2.2 | Jet Mass Templates | 29 |

| | | |
|-----------|---------------------------------|-----------|
| 9.3 | Constructing a Search | 29 |
| 9.3.1 | Background Estimates | 29 |
| 9.3.2 | Limits | 29 |
| 9.3.3 | Future Prospects | 29 |
| 10 | Conclusions | 30 |
| A | A Long Proof | 31 |
| | Bibliography | 32 |

List of Tables

List of Figures

| | | |
|------|---|----|
| 5.1 | An aerial view of Geneva, with the location of the LHC superimposed. The individual detectors (described in chapter 6, as well as the main CERN Meyrin site, are also highlighted. Image courtesy CERN. | 6 |
| 5.2 | A schematic drawing of the initial design of a shared LEP/LHC tunnel, with the LHC beamline positioned on top of the existing LEP beamline [1]. | 8 |
| 5.3 | A photo of the final LHC tunnel, no LEP beamline, in contrast to the first plans shown in Figure 5.1. Photo courtesy of USLHC. | 9 |
| 6.1 | A schematic diagram of the interactions of various particles with detector components. Copyright CERN. | 12 |
| 6.2 | A computer-generated view of the ATLAS detector, with people for scale. Copyright CERN. | 13 |
| 6.3 | An early view of a potential superconducting air-core toroid magnet system for the ATLAS detector from the 1992 Letter of Intent [2]. | 15 |
| 6.4 | A photograph of the ATLAS solenoid shortly after the winding of the coils was finished. Copyright CERN. | 16 |
| 6.5 | A photograph of the ATLAS barrel toroids after their installation. Note person in the center for scale. Copyright CERN. | 17 |
| 6.6 | A photograph of an ATLAS endcap toroid shortly before its installation in the detector. Copyright CERN. | 17 |
| 6.7 | A computer-generated view of the ATLAS inner detector, with relevant sizes of the detector marked out. Copyright CERN. | 18 |
| 6.8 | A cut-out view of the ATLAS inner detector, showing the layers a particle would interact with as it passed outward from the collision point. Copyright CERN. | 19 |
| 6.9 | A computer-generated view of the ATLAS pixel detector. Copyright CERN. | 21 |
| 6.10 | A photograph of one segment of the ATLAS SCT endcap disks. Copyright CERN. . | 22 |
| 6.11 | A photograph of the ATLAS TRT system during testing. Copyright CERN. | 23 |

| | |
|--|----|
| 6.12 A computer generated image of the ATLAS calorimeter system, showing the locations of each different subdetector. Copyright CERN. | 24 |
| 6.13 A photograph of the accordion structure used in the LAr barrel. Copyright CERN. . | 24 |
| 6.14 A photograph of the LAr endcap after installation in the cryostat system. Copyright CERN. | 25 |
| 6.15 A photograph of one of the scintillating tiles which give the tile calorimeter its name. Copyright CERN. | 25 |
| 6.16 A photograph of the installation of the barrel tile calorimeter. Copyright CERN. . | 26 |
| 6.17 A computer generated image showing the locations of each of the muon spectrometer subsystems. Copyright CERN. | 26 |

Chapter 1

Introduction

...

Chapter 2

The Standard Model, and the Theory of Strong Interactions

2.1 Overview

2.2 Spontaneous Symmetry Breaking, the Electroweak Force, and the Origin of Mass

2.3 Quantum Chromodynamics and Strong Interactions

Chapter 3

Jets and Substructure

3.1 The Goal of Jets, and Jet Algorithms

3.2 Jet Substructure: Going Deeper

3.3 Calculations with Jets

Chapter 4

Supersymmetry, R -Parity, and Naturalness

4.1 The Problem of the Standard Model

4.2 Supersymmetry: The Solution?

4.3 R -Parity, and How to Violate It

4.4 Naturalness, or the Pursuit of Beauty

...

Chapter 5

The Large Hadron Collider

The Large Hadron Collider (LHC) is a 27 km long proton-proton (pp) synchotron built on the border of France and Switzerland, near the city of Geneva. The accelerator is nestled beneath mostly bucolic French farmland, as seen in Figure 5.

The total costs of the accelerator and the detectors it serves are estimated at \$20 billion, making the LHC one of the largest scientific enterprises ever attempted. [*Ed: cite this*] The project is full of similar superlatives: the accelerator is the largest machine, the ATLAS detector is the largest detector, the CMS detector is the heaviest. 10,000 scientists from 113 countries work on some aspect of the project, making it one of the best examples of international cooperation that mankind has produced.

The machine is composed of eight essentially identical sectors,

The machine was designed to deliver collisions at $\sqrt{s} = 14$ TeV energy at a rate of 10^{34} cm $^{-2}$ /s, but as of 2012 collisions had only occurred at 8 TeV and a rate of 5×10^{33} cm $^{-2}$ /s.

[*Ed: Describe sectors, luminosity, energy, helium*]

5.1 History

The LHC was first discussed publically at the ECFA-CERN Workshop held at Lausanne and Geneva in March of 1984 [1]¹. This was a very active time for proposing new collider experiments, as extensive work on the 40 TeV pp Superconducting Supercollider (to be built in Waxahachie, Texas) had recently displaced a proposal for a 4 TeV $p\bar{p}$ Dedicated Collider at Fermilab [1, 3], though construction continued on Fermilab's 2 TeV $p\bar{p}$ Tevatron collider. The Soviet Union was even planning a 6 TeV $p\bar{b}$ collider, the Accelerator and Storage Complex (UNK) [4][*Ed: This needs a better citation*]. In this busy landscape, the proposal of another machine at CERN– which was currently building the Large Electron Positron (LEP), the world's largest e^+/e^- collider– was very ambitious indeed.

¹4 years and 1 month before the author was born!



Figure 5.1: An aerial view of Geneva, with the location of the LHC superimposed. The individual detectors (described in chapter 6, as well as the main CERN Meyrin site, are also highlighted. Image courtesy CERN.

Several characteristics made the proposed LHC unique and worth pursuing in such a competitive environment. First, with the construction of the LEP tunnel on track for completion in 1988, the civil-engineering component of the project was greatly reduced, especially compared to the enormous expense of constructing the SSC tunnel. Second, while the design goals of 20 TeV collisions were at a significantly lower energy than the SSC, the projected luminosity was eventually designed to be a factor of 10 higher ($10^{34} \text{ cm}^{-2}/\text{s}$, though the initial designs focused on $10^{33} \text{ cm}^{-2}/\text{s}$) and so the LHC could potentially gain sensitivity by accumulating data more quickly. Finally, as figure 5.1 shows, the initial designs for the LHC envisaged the LHC beamlines actually sitting on top of the existing LEP beamlines. The resulting hybrid collider would be able to run pp , ep , and ee collisions. This would not only extend the reach of the physics program by allowing for the study of deep inelastic scattering at higher energies than the HERA collider at DESY [*Ed: Cite this– HERA and e/p if possible.*], but would also allow for the study of Z bosons from ee , which could potentially be used as a calibration source for detectors before pp collisions [1].

With the approval of the SSC in 1987 and the subsequent start of construction in 1991, CERN was mostly focused on the construction and operation of LEP but did not stop planning for the LHC. This proved remarkably prescient, as in the face of changing budget priorities and the end of the Cold War, the SSC ended up being cancelled in 1993. [*Ed: This probably needs citations.*] CERN, on the other hand, approved a staged construction plan for the LHC in 1994, targetting first 10 TeV collisions in 2004 and then 14 TeV in 2008. Japan and the US joined CERN as observer states in 1995 and 1997 respectively, each contributing significantly to the construction of the LHC and joining the physics program of CERN.*[Ed: Statement about internation collaboration, compared to SSC? Statement about the 10 TeV plan being dropped?]*

The Conceptual Design Report [5] published in 1995 reflected the changed landscape with the demise of the SSC and the results of more detailed cost estimates. The design energy was lowered to 14 TeV– higher energies would have required more costly magnets– while the design luminosity was actually increased to $10^{34} \text{ cm}^{-2}/\text{s}$. This increase in luminosity came at a cost: the number of interaction points was reduced to four instead of eight, and only two would receive collisions at a high rate. [*Ed: Mention pileup here or no?*] Critically, it was also decided to remove the LEP beamline and magnets, as it was deemed too costly to follow the existing LEP infrastructure. While this reduced the physics program of the LHC substantially, being the only high energy hadron collider was still a rather broad portfolio.

With the shutdown of LEP in 2001², the construction of the LHC began in earnest. It would take till 2007 to install the last magnet in the LHC, and the detectors finalized their own installations only in 2008. Figure 5.1 shows the final state of the LHC tunnel (without the originally planned LEP beamline). The first low-energy collisions occurred on September 10, 2008, putting the LHC almost on track of its initial goal of 14 TeV collisions in 2008. [*Ed: Probably want to add a bit more*

²Not without controversy, as there was perhaps a tantalizing sign of an excess in Higgs-boson like events during the final runs of LEP.*[Ed: cite me]*

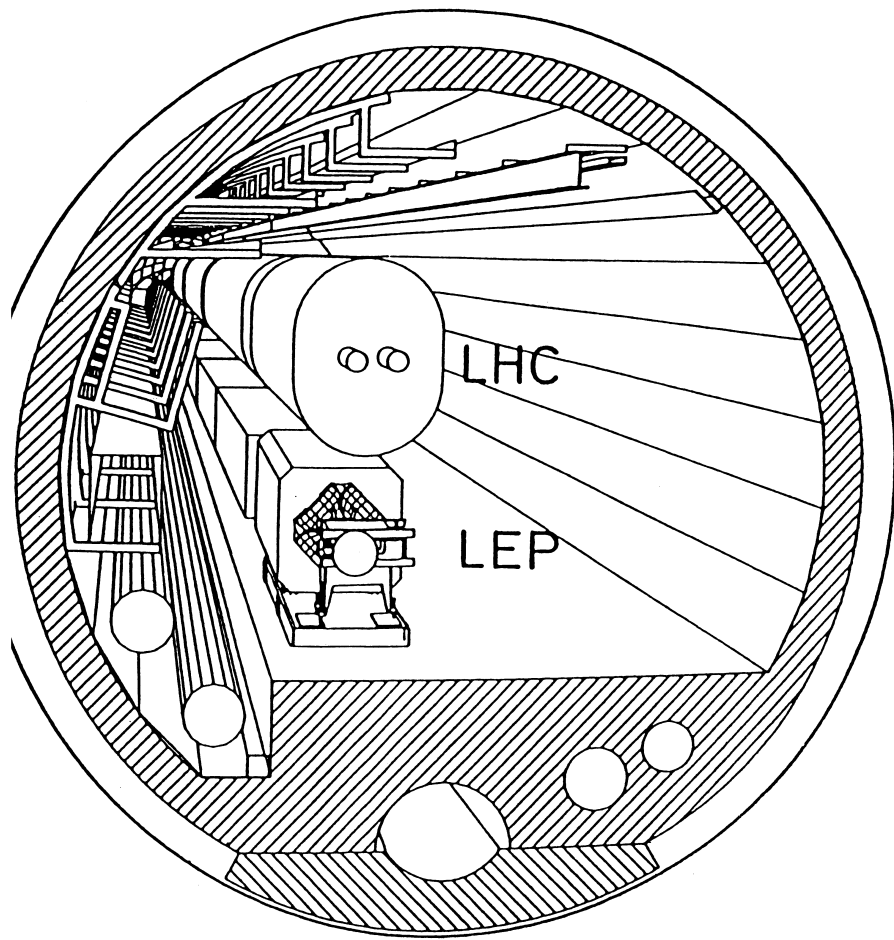


Figure 5.2: A schematic drawing of the initial design of a shared LEP/LHC tunnel, with the LHC beamline positioned on top of the existing LEP beamline [1].



Figure 5.3: A photo of the final LHC tunnel, no LEP beamline, in contrast to the first plans shown in Figure 5.1. Photo courtesy of USLHC.

on construction.]

However, an “incident” on September 19 ended up delaying the full startup for a year [6]. On that day, the operators were testing the last sector of the LHC at current levels appropriate for 5.5 TeV beams. A resistive zone developed in the electrical bus connection between a dipole and quadrupole magnet. While the power supply detected this and shut down within 0.39 seconds and the quench protection circuitry began to engage at 0.89 seconds, it was already too late: an electrical arc had sparked and punctured the liquid helium enclosure and the insulation vacuum along the cryostat. This, along with the electrical noise induced by the power supply shutdown and the heat dissipation caused by the quench protection circuitry, triggered a chain reaction in which several other magnets also began to quench and other vacuum systems were degraded. As the helium began to escape the cryostat, pressure relief valves correctly opened and vented the helium to atmosphere. However, an additional complication proved to be a problem: neighboring subsectors had their vacuum systems separated by vacuum barriers, meant to isolate the vacuum systems of neighboring areas. The vacuum barriers could only sustain a rather low pressure difference, and the extreme pressures generated by the evacuating helium overwhelmed these connections. The attendant large

pressure forces ended up displacing dipoles from their support structures, and knocked the cryostats from their support jacks— in some cases even ripping the anchors from the concrete floor. A total of six tons of helium, five quadrupoles, and twenty-four dipoles were lost in the incident.

Collisions would begin in earnest at a lowered energy of 7 TeV in 2010 and 2011. After two years of successful and safe operations at the reduced energy, 2012 saw a large increase in luminosity and an increase of the collision energy to 8 TeV. [*Ed: A bit more on operations at 8 TeV*.] The LHC then proceeded to shut down in 2013 until mid-2015 for a further round of repairs and consolidations of electrical connections to guarantee the safety of operations at near the design energy. As the restart of the LHC approaches in the coming months, we are anticipating collisions at 13 TeV with luminosity likewise reaching near design levels. The LHC will have broken energy records twice in the span of five years, making this an incredibly exciting time to be working in particle physics.

5.2 Machine Design

5.3 Luminosity, and Pileup

5.4 Operations in 2010-2012

Chapter 6

The ATLAS Detector

The design of the LHC, with two high-luminosity interaction points at opposite ends of the ring, called for two general purpose detectors to be built in these locations. Their charge was to accurately reconstruct collision events in the most hostile conditions yet seen in a collider: with a bunch spacing of 25 ns and the unprecedented introduction of pile-up the detectors would have an enormous challenge ahead of them in dealing with both the rate and the reconstruction of events. ATLAS (A Toroidal LHC APparatus) [7] and CMS (Compact Muon Solenoid) [8] were the two detectors built for this task, with ATLAS occupying the (much more convenient) Point 1 and CMS located at the (very distant) Point 5. The data presented in this thesis was collected by the ATLAS experiment in pp collisions at $\sqrt{s} = 8$ TeV in 2012.

Particle detectors measure particles via their interactions with matter, as drawn schematically in Figure 6. For example, charged particles (such as electrons and some hadrons) interact electromagnetically with silicon and gas tubes, leaving hits in different layers of detectors which can be traced back to form a track. Electrons and photons, with their low masses and high rate of interaction with matter, are measured by the electromagnetic calorimeter. The calorimeter is composed of alternating layers of metal meant to cause the particle to interact and lose energy, and active materials which measure the energy left behind in these interactions. The hadron calorimeter follows a similar principle, and alternately placed layers of metal and active material again aim to stop and measure the hadrons which the electromagnetic calorimeter did not stop. Muons, which do not interact very much with matter most matter but do leave hits in trackers, survive past even the hadronic calorimeter, and a special set of muon detectors can be used to identify them there. Neutrinos, as they interact with matter only via the weak force and thus very rarely, escape detection and are reconstructed only by inferring their presence from the lack of momentum conservation in the transverse plane.

A significant constraint in the design of detectors is the interaction of particles with matter. [**Ed:** *This needs citations.*]

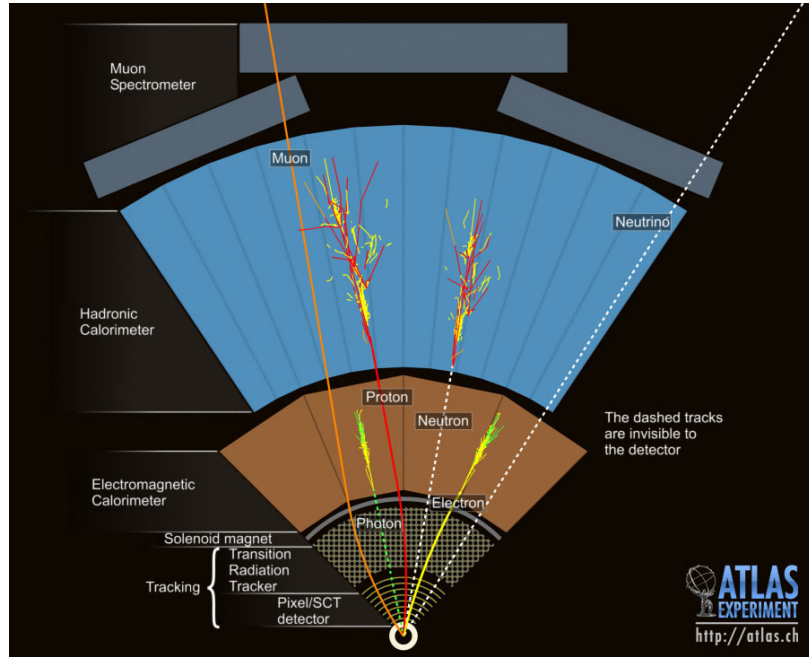


Figure 6.1: A schematic diagram of the interactions of various particles with detector components.
Copyright CERN.

General purpose particle detectors thus demand the following characteristics: [Ed: *define radiation lengths? above?*]

1. Tracking systems must be able to identify primary and secondary vertices, while minimizing the radiation lengths before the calorimeters
2. Strong calorimetry systems are required to accurately measure the energy and position electrons, photons, and hadrons
3. Muon systems must be able to precisely reconstruct muons

To this end, the ATLAS detector is built in the traditional onion-layer configuration, which measures particles as they travel perpendicular to the beam. The Inner Detector, composed of the concentric Pixel, SCT [Ed: *define*], and Transition-Radiation-Tracker (TRT) subsystems, lies at the center of the detector and precisely measures tracks created by charged particles. A 2 T solenoid encloses the Inner Detector, bending charged particles and enabling the measurement of their momenta. Next the Electromagnetic Calorimeter (ECal), composed of liquid argon (LAr) and copper, sits outside of the solenoid in a liquid nitrogen cryostat, and measures energy deposits from electrons and photons (as well as hadrons to a lesser extent). The Hadronic Calorimeter, built to measure and stop any remaining hadronic particles, is composed of steel and scintillating tile in the

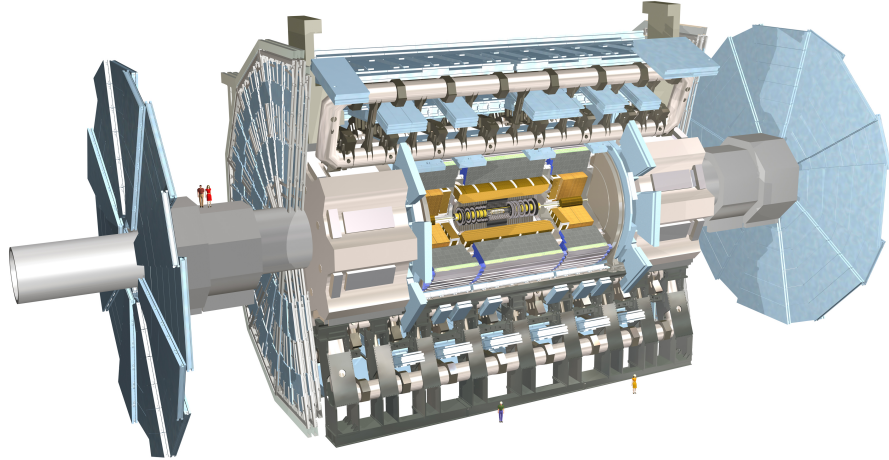


Figure 6.2: A computer-generated view of the ATLAS detector, with people for scale. Copyright CERN.

center (referred to as the barrel), and LAr and copper in forward regions (referred to as end-caps). Surrounding these are an additional set of magnets: the superconducting air-core toroids of the barrel and endcaps, which bend particles in the plane perpendicular to that of the bending due to the solenoid. [Ed: *That needs cleaning.*] The Muon Spectrometer (composed of MDT, RPC, TGC, and CSC subsystems) sits outside of (and next to) these magnets, and provides a final measurement of the charged particles which reach that far. The entire detector is shown in Figure 6. The incredible size of the detector—25 m in diameter, and 46 m long—is dominated by the Muon Spectrometer and the toroids. On the other hand, the detector is comparatively light (only 7000 tons, compared to 14,000 tons for CMS), as the air-core toroids do not add substantial weight to the detector. [Ed: *decide how to cite all this*]

In keeping with the principle of “similar, but opposite” established by their locations, the ATLAS and CMS detectors take complementary approaches to the various aspects of event reconstruction in collisions. All general purpose detectors have the same basic goals: they must reconstruct the outgoing, stable particles produced in collisions and the subsequent decays of particles in these collisions. Different particles are detected with different general classes of detectors, of which there are many possible types. For example, electrons and photons are measured by the ECal, for which

ATLAS used a liquid argon (LAr) and copper system while CMS used a crystal lead tungstate system. Each had their own advantages and disadvantages (ATLAS's was less costly and already proven technology with better position resolution, while CMS took a riskier route which promised better energy resolution), but overall performance between the detectors tends to be very similar because of various trade-offs. In the case of the ECals, the precision of ATLAS and CMS's $H \rightarrow \gamma\gamma$ measurements ended up being largely similar [*Ed: cite?*], in no small part because CMS's all-silicon tracking system introduced greater radiation lengths before the calorimeters, thereby prompting more photons to convert and losing precision in the measurement. On the other hand, CMS's comparatively weak brass hadronic calorimeter (compared to ATLAS's higher resolution tile calorimeter), is compensated by their tracking system, which enables a particle-flow reconstruction algorithm to combine information from all detectors and improve jet performance to levels very similar to ATLAS. [*Ed: consider citations, and substantial revisions here*]. Similarly, the large size and extra toroid magnets of ATLAS allow for a larger lever-arm and an additional set of measurements of muons (enabling reconstruction with or without the inner detector): however, muon reconstruction performance in CMS is very similar because the stronger solenoidal magnetic field (4 T compared to 2 T) allows for a better measurement using the inner detector only (with the muon systems on CMS providing only a tag of a passing muon, and not a complete reconstruction).

6.1 History

The first public discussion of the proposals which became the ATLAS detector occurred in 1992 at the General Meeting on LHC Physics at Evian-les-Bains [9, 10]. At the time, four general purpose detectors (much like the four detector configuration in place at LEP) were seriously considered: EAGLE, ASCOT, CMS, and L3 (as an upgrade to the existing LEP detector, including a movable stage which would allow it to take data from both e^+e^- and pp collisions). Several additional single purpose (heavy ion, neutrino, and B -physics) detectors were also proposed.

ATLAS emerged in a later 1992 Letter of Intent as a merger of the ASCOT and EAGLE collaborations [2]. ASCOT (Apparatus with SuperCOnducting Toroids) contributed the physically-defining feature of the secondary toroidal magnet system and standalone muon measurement system, as well as the tradition of using a tortured amalgamation of letters to form a name. EAGLE (Experiment for Accurate Gamma, Lepton and Energy measurements) on the other hand featured a stronger 2 T magnetic field, and inner-detector and calorimeter designs more similar to some of the final ATLAS systems. The detector described in the Letter of Intent already resembled ATLAS in many important ways, featuring the superconducting air-core toroids, accordion-shaped liquid Argon electromagnetic calorimeters, scintillating tile hadron calorimeters, and multi-design inner detector. 6.1 shows an early drawing of ATLAS from the Letter, and already the detector looks recognizable to its current form.

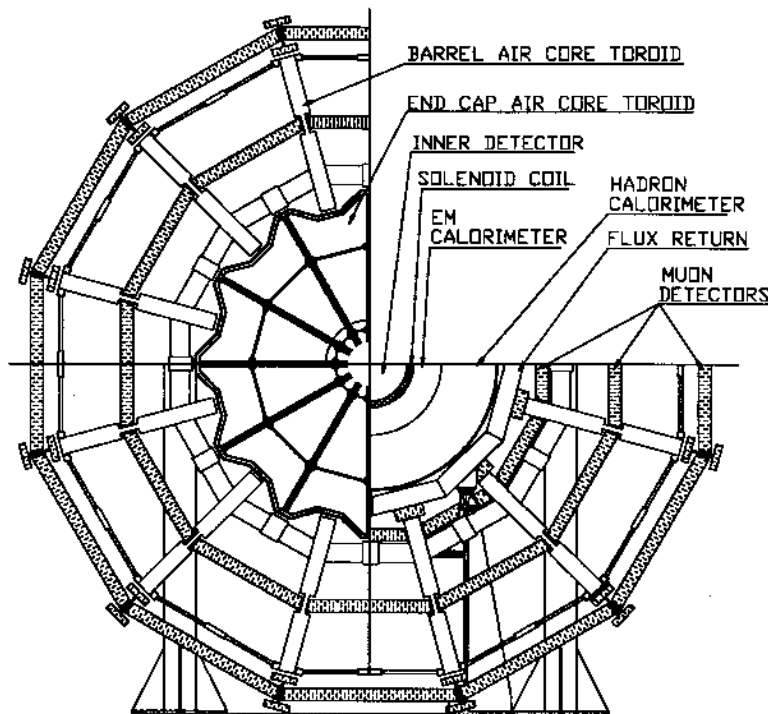


Figure 6.3: An early view of a potential superconducting air-core toroid magnet system for the ATLAS detector from the 1992 Letter of Intent [2].



Figure 6.4: A photograph of the ATLAS solenoid shortly after the winding of the coils was finished.
Copyright CERN.

6.2 Magnet Systems

6.2.1 Solenoid

6.2.2 Toroids

6.3 Inner Detector

The ATLAS Inner Detector (ID) sits at the center of the experiment [7]. The purpose of the detector is to reconstruct the tracks (i.e. trajectories) of charged particles produced by the collisions of the LHC in order to not only accurately measure the locations of primary and secondary vertices, but to also directly measure the momenta and locations of charged particles [11]. The detector covers the range $|\eta| < 2.5$, and is capable of measuring particle momenta as low as $p_T = 500$ MeV. Charged particle reconstruction efficiencies are typically greater than 90% for 100 GeV particles and 70% for 1 GeV particles, with a strong η dependence. Typical p_T resolutions are of order $0.05\% \text{GeV}^{-1} \times p_T \oplus 1\%$, and impact parameter resolutions are approximately $10 \mu\text{m}$ ¹.

The ID is composed of several independent detector subsystem which read out the locations of interactions with charged particles. These hits are fit to tracks by a suite of tools, which include standard global- χ^2 and Kalman-filters, but also several specialized fitters [11]. The p_T of the particles is obtained by measuring the curvature produced by the 2 T solenoid (as described

¹The impact parameter is the perpendicular distance from the origin to the point of closest approach of the track, and is critical for the measurement of secondary vertices.

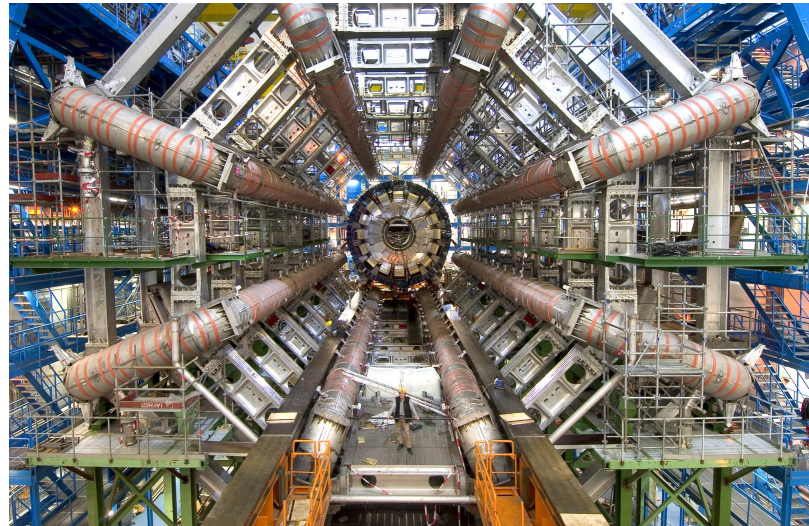


Figure 6.5: A photograph of the ATLAS barrel toroids after their installation. Note person in the center for scale. Copyright CERN.



Figure 6.6: A photograph of an ATLAS endcap toroid shortly before its installation in the detector. Copyright CERN.

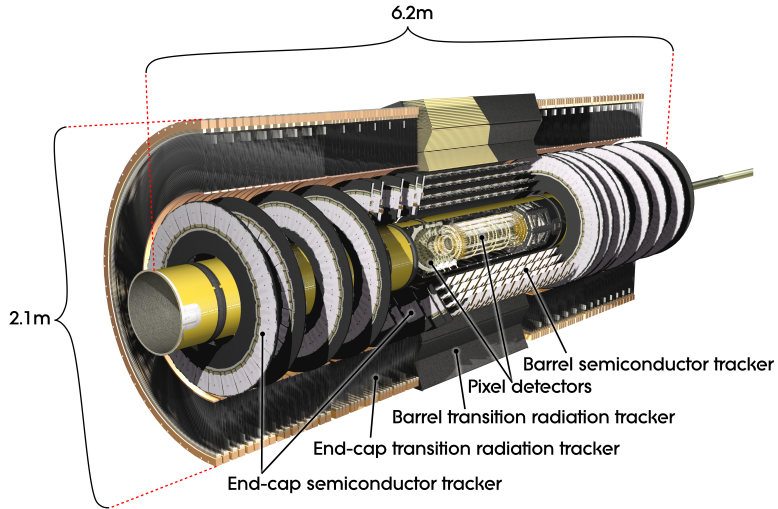


Figure 6.7: A computer-generated view of the ATLAS inner detector, with relevant sizes of the detector marked out. Copyright CERN.

by Section 6.2.1) surrounding the detector. The three subsystems, described below, are the silicon pixel tracker (Pixel), silicon microstrip tracker (SCT), and transition radiation tracker (TRT). The combined detector has a length of 7024 m and a radius of 1.15 m [7]. Figure 6.3 shows a computer generated image of the combined ID, and Figure 6.3 shows a computer-generated image of the various subcomponents of the ID and their spacing.

At design luminosity, the detector is expected to measure approximately 1000 charged particles every 25 ns within the detector acceptance [11]. The added growth of pileup in the 2012 and future LHC runs have increased the importance of the Inner Detector as the primary vertex identification has become even more critical [12], but growing challenges from the computing time necessary to fit so many tracks (which increase more than quadratically as the number of detector hits [13]) will also need to be overcome to make best use of the detector's information.

6.3.1 Silicon Pixel Detector

The innermost ATLAS sub-detector is the Silicon Pixel Detector [7]. The principal of detection for the pixel detector follows the standard ionizing radiation detector [14]. Charged particles interact with the active medium (doped silicon), knocking electrons loose from their host atoms and creating electron-hole pairs. An applied voltage carries the holes and electrons to opposite ends of the detectors, where they are read out. The active regions are very small in both x and y dimensions, allowing for many independent measurement channels in a small area. Given the high number of particles expected from LHC collisions, and that the density is greatest nearest to the interaction

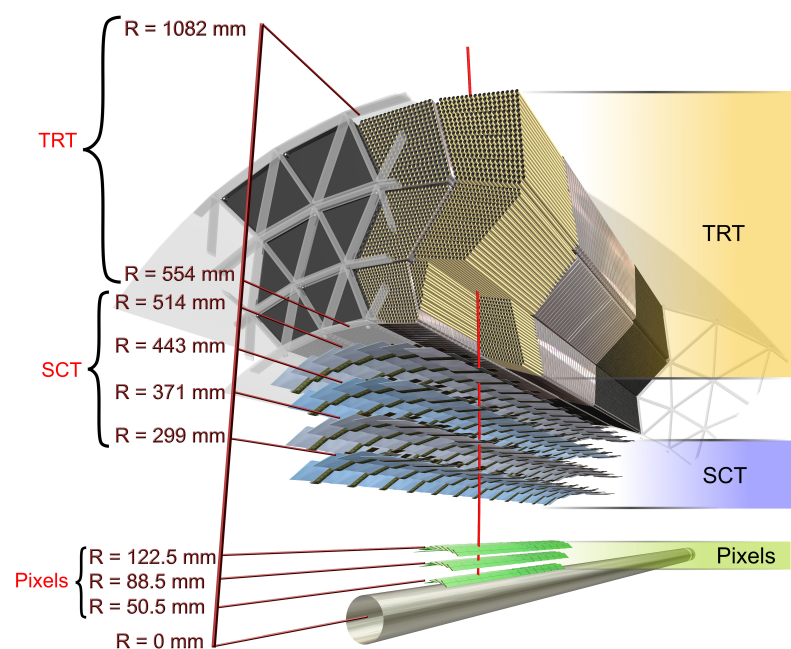


Figure 6.8: A cut-out view of the ATLAS inner detector, showing the layers a particle would interact with as it passed outward from the collision point. Copyright CERN.

point, it is critical that the innermost detector have a huge number of very small channels, making the task perfectly suited for a pixel detector.

80.4 million independent pixel channels, with a size of $50 \times 400 \mu\text{m}$, are read out by 1744 bump-bonded modules attached to the active sensors. Each of the modules are composed of 16 radiation hard front-end chips [7]. This corresponds to a combined active area of 1.7 m^2 . The detector is arranged in three radial layers in the barrel section, and three disks in the end-caps. In the radial layers, the pixels have a resolution of $10 \times 115 \mu\text{m}$ in $R - \phi$ and z respectively, and in the end-caps the orientation is perpendicular and the resolution is $10 \times 115 \mu\text{m}$ in R and $R - \phi$: the orientations are always chosen such that the most precise measurement takes place in the direction most relevant to the measurement of the track p_T .² The barrel and disk arrangement is shown in Figure 6.3.1. Hits are read out when charge has been collected over a tunable threshold determined by the noise of each pixel, resulting in typical occupancies of $10^{-4} - 10^{-5}$, though this grows obviously grows with additional pp interactions.

The innermost radial layer, known as the *b*-layer, sits only 50.5 mm from the center of the beampipe, while the outermost layer is located at 122.5 mm [7]. By placing detectors so close to the interaction point, it is possible to very accurately measure the location of both primary vertices—the locations of pp collisions—and second vertices—the locations of the displaced decays of particles with long lifetimes, such as *B*-hadrons [11].

Placing the detector so close to the beamline comes at a price, however, as the detector is particularly susceptible to radiation damage due to the high flux of particles through a small area. At design luminosity, this is expected to be about 158 kGy/year at the *b*-layer, reduced to 25.4 kGy/year at the outermost layer [7]. Damage comes in the form of displaced atoms in the doped silicon lattice, resulting in lower electron-hole yields per particle interaction. Some of the damage is mitigated by operating at cold temperatures (typically -5 to -10° C), and higher bias voltages can also alleviate the effects.

While the entire Inner Detector is expected to be replaced after 300 fb^{-1} are collected in order to replace the damaged components, the long shutdown of 2013-2015 presented ATLAS with the opportunity to augment the existing pixel detector with the so-called Insertable B-Layer (or IBL) [15]. The IBL, which adds an additional layer of pixels to the barrel and endcap pixel systems, is attached directly to a new carbon-fiber beampipe, and is located only 33 mm from the center of the beampipe. Due to this extremely close distance, the pixel size has been further reduced to $50 \times 250 \mu\text{m}$. The vertexing performance (especially secondary vertex identification for *b*-tagging) of ATLAS in Run 2, starting in 2015, is expected to substantially increase due to the IBL.

²The $R - \phi$ coordinate is simply a distance-projected version of the azimuthal angle ϕ .

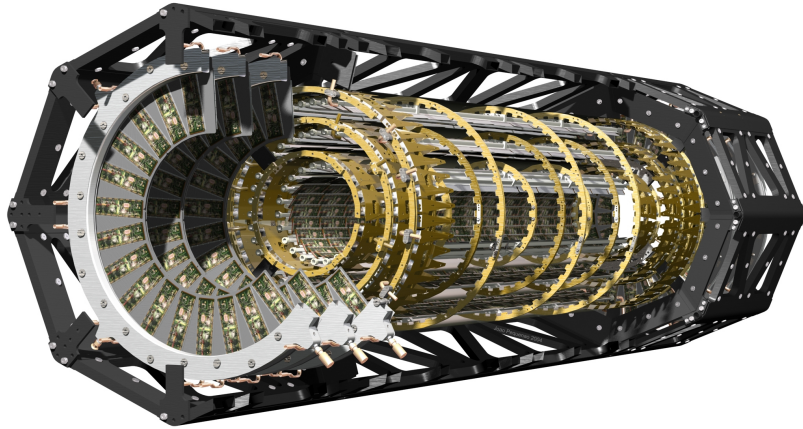


Figure 6.9: A computer-generated view of the ATLAS pixel detector. Copyright CERN.

6.3.2 Silicon Strip Tracker

The next outermost subdetector in the ID is composed of silicon microstrip layers [7], and is commonly referred to as the SCT. The SCT operates under a very similar principle to the Pixel detector: doped silicon under an electric bias is the active medium, and electron/hole pairs are collected to read out hits. Unlike the Pixels, one dimension of the detector is ganged together to form the eponymous strips. Two sets of detectors must therefore placed perpendicularly to each other (or at some other angle) to provide a true two-dimensional measurement, but the number of channels to be read out has been significantly reduced [14].

The ATLAS SCT contains 4088 modules, each composed of two 64 mm silicon strip sensors with a 40-mrad angular offset [7]. Like the Pixels, the detector is arranged into radial layers in the barrel and disks in the endcap, of which there are 4 and 9 respectively. The strips have a resolution of 17×580 in $R - \phi$ and z respectively in the barrel, and 17×580 in $R - \phi$ and R in the disks. The SCT occupies the space between 275 mm and 560 mm from the beamline. The detector contains a total of 6.3 million read out channels read out by radiation hard front-end chips [16]. The increased distance of the SCT from the beamline significantly lowers the rate of expected radiation damage, but increased bias voltages are still expected to be necessary after significant luminosity [7]. Figure 6.3.2 shows one segment of the SCT endcap disks.

6.3.3 Transition Radiation Tracker

The final subdetector of the ID is the transition radiation tracker [7]. Unlike the other subdetectors of the ID, the TRT is not made out of silicon: instead, it is composed of 2 mm (in radius) straw tubes (proportional drift tubes) [7]. [*Ed: Discussion of principals, once I have the book.*]

The TRT covers the range $|\eta| < 2.0$ in the standard barrel and endcap arrangements [17]. There

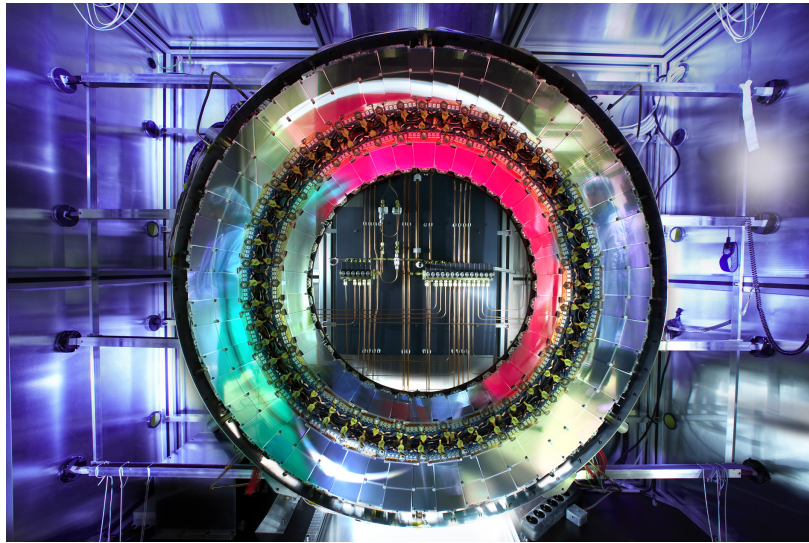


Figure 6.10: A photograph of one segment of the ATLAS SCT endcap disks. Copyright CERN.

are 52544 tubes, each 1.44 m in length, arranged in two active regions on either side of the center of the detector. The endcaps are each composed of 122880 370 mm long tubes, organized into 18 wheels. The barrel is arranged in layers of 76 straws, while the endcaps have 160 planes. There are a combined 350848 channels in the detector.

The TRT, whose active elements are much larger than that of the silicon sensors in the rest of the ID, has a significantly larger hit resolution: $130 \mu\text{m}$ in $R - \phi$ [7]. This is partly compensated by the large number of straws that charged particles cross, generating on average 30 hits [11]. The TRT has the added benefit of providing identification of electrons via the emission of transition X-rays. [*Ed: Few sentences on how this works.*] In the barrel, the TRT straws are embedded in a set of polypropylene-polyethylene fibers with a diameter of $19 \mu\text{m}$; in the endcap, foil is interleaved between the straws. A special readout system in the straw readout electronics measures these transition photons [18]. This type of identification is not possible with silicon detectors, providing the TRT with a unique capability. Finally, the gas tubes of the TRT present a significantly lower amount of material to particles traversing the ID compared to silicon detectors, thereby degrading less the performance of the ECal and HCal.

Given the distance of the TRT from the interaction point, and the greater resilience of gas tubes to radiation compared to silicon (there is no atomic lattice to be damaged), the TRT is not expected to be significantly damaged during the course of data-taking. However, with the presence of increasing pileup conditions in upcoming runs, the occupancy of the TRT is expected to grow significantly, presenting a significant challenge to continued operation [19].

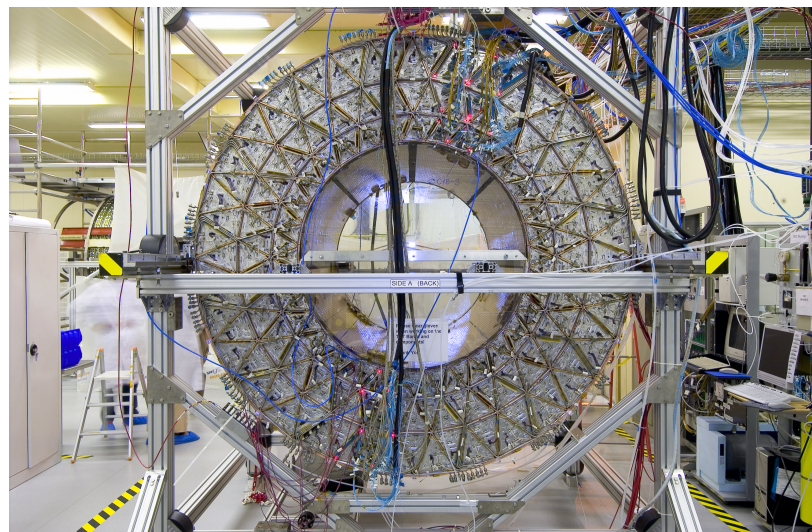


Figure 6.11: A photograph of the ATLAS TRT system during testing. Copyright CERN.

6.4 Calorimeters

6.4.1 Electromagnetic Calorimeter

6.4.2 Hadron Calorimeter

6.5 Muon Spectrometer

6.6 Triggering

6.7 Data Quality

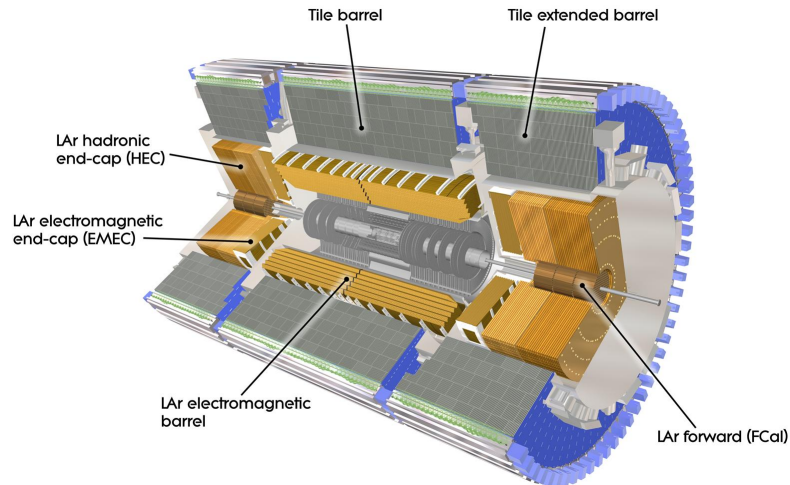


Figure 6.12: A computer generated image of the ATLAS calorimeter system, showing the locations of each different subdetector. Copyright CERN.

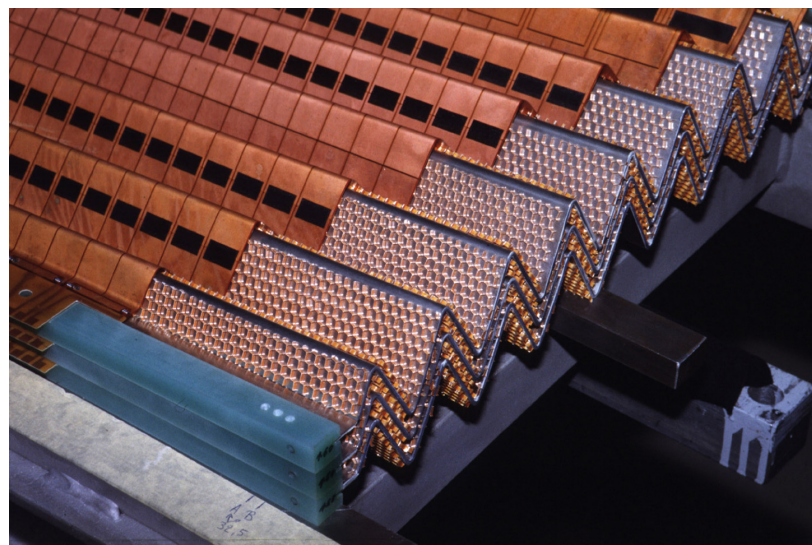


Figure 6.13: A photograph of the accordion structure used in the LAr barrel. Copyright CERN.

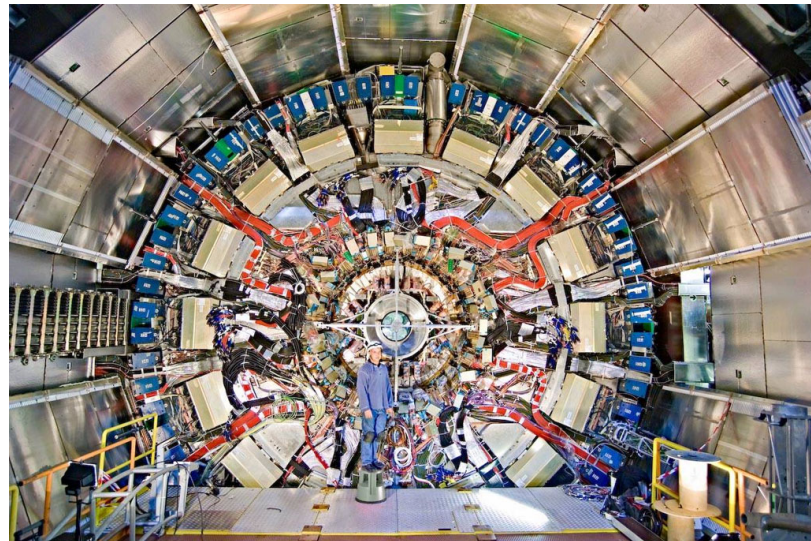


Figure 6.14: A photograph of the LAr endcap after installation in the cryostat system. Copyright CERN.

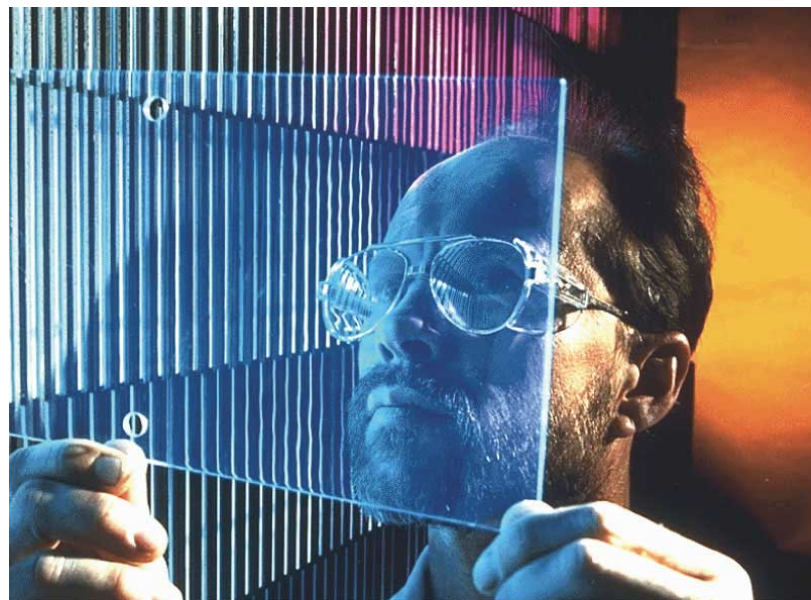


Figure 6.15: A photograph of one of the scintillating tiles which give the tile calorimeter its name. Copyright CERN.

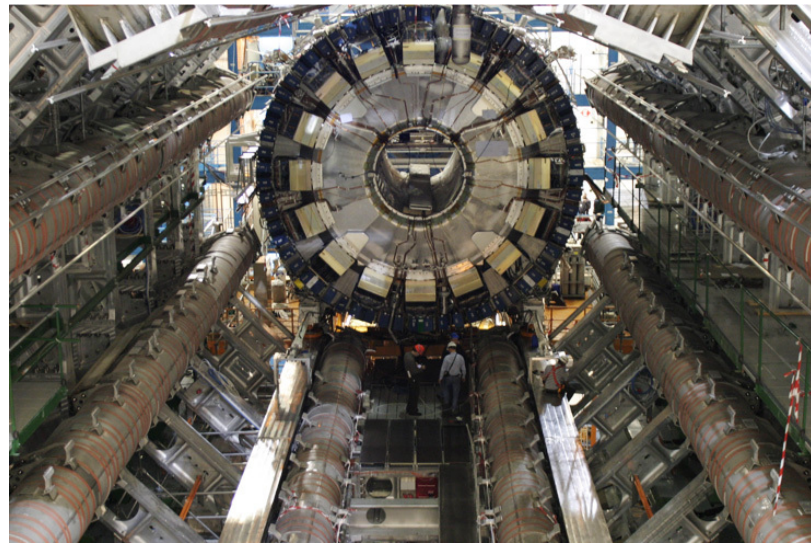


Figure 6.16: A photograph of the installation of the barrel tile calorimeter. Copyright CERN.

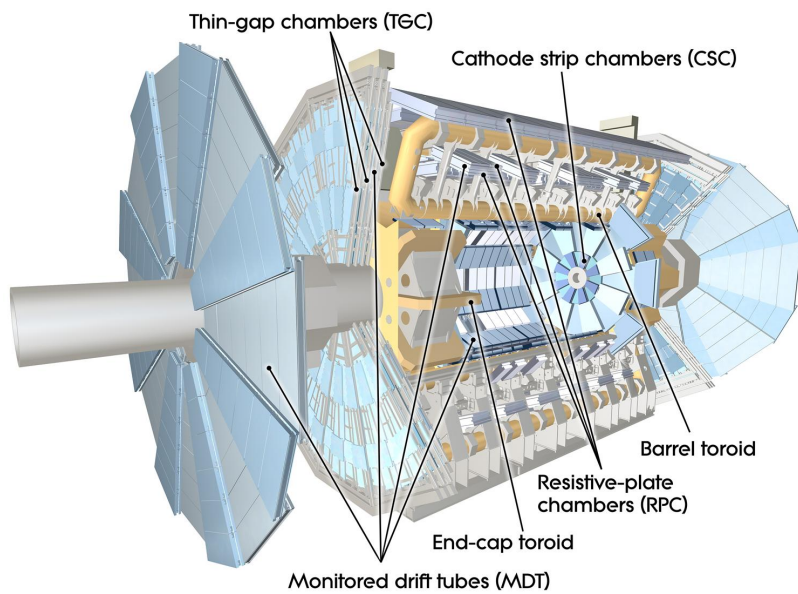


Figure 6.17: A computer generated image showing the locations of each of the muon spectrometer subsystems. Copyright CERN.

Chapter 7

Jet Reconstruction with ATLAS

7.1 Clusters, Towers, and Tracks, Oh My

7.1.1 Cluster Calibration

7.2 Jet Calibration

7.3 Quark/Gluon Discrimination

7.3.1 Lots of subsections

...

Chapter 8

Seeing Color at the LHC

8.1 Motivation

8.2 Reconstructing Color

8.2.1 Finding Top Quarks

8.2.2 Origin Corrections

8.2.3 Resolution Effects

8.2.4 Track and Cluster Uncertainties

8.3 Measuring Color

8.3.1 Unfolding

8.3.2 Results

8.3.3 Future Prospects

...

Chapter 9

Searching for Supersymmetry with Super Jets

9.1 Motivation

9.2 Why Jet Substructure?

9.2.1 Total Jet Mass, and Other Variables

9.2.2 Jet Mass Templates

9.3 Constructing a Search

9.3.1 Background Estimates

9.3.2 Limits

9.3.3 Future Prospects

...

Chapter 10

Conclusions

...

Appendix A

A Long Proof

...

Bibliography

- [1] CERN, *Large Hadron Collider in the LEP Tunnel*, vol. 1. March, 1984.
<https://cds.cern.ch/record/154938?ln=en>.
- [2] ATLAS Collaboration, *ATLAS: letter of intent for a general-purpose pp experiment at the large hadron collider at CERN*. Letter of Intent. CERN, Geneva, 1992.
<https://cds.cern.ch/record/291061>.
- [3] *Proposal for a Dedicated Collider at the Fermi National Accelerator Laboratory*, tech. rep., Fermilab, 1983. <http://lss.fnal.gov/archive/misc/fermilab-misc-1983-02-02.pdf>.
- [4] *Perestroika and Particle Physics*, Science News (1988) .
<http://www.thefreelibrary.com/Perestroika+and+particle+physics.-a06519299>.
- [5] LHC Study Group Collaboration, T. S. Pettersson and P. Lefèvre, *The Large Hadron Collider Conceptual Design*, Tech. Rep. CERN-AC-95-05-LHC, CERN, Oct, 1995.
<https://cds.cern.ch/record/291782>.
- [6] M. Bajko et al., *Report of the Task Force on the Incident of 19th September 2008 at the LHC*, Tech. Rep. CERN-LHC-PROJECT-Report-1168, CERN, Geneva, Mar, 2009.
<https://cds.cern.ch/record/1168025>.
- [7] ATLAS Collaboration, *The ATLAS Experiment at the CERN Large Hadron Collider*, JINST **3** (2008) S08003.
- [8] CMS Collaboration, *The CMS experiment at the CERN LHC*, JINST **3** (2008) S08004.
- [9] European Committee for Future Accelerators and European Organization for Nuclear Research, *Towards the LHC Experimental Programme: 5-8 March 1992, Evian-les-Bains, France : LHC : Proceedings of the General Meeting on LHC Physics & Detectors*. CERN, 1992. <https://cds.cern.ch/record/236265/>.
- [10] *Early days: The Evian experiment meeting (archive)*, CERN Courier (2008) .
<http://cerncourier.com/cws/article/cern/35867>.

- [11] ATLAS Collaboration, *Expected Performance of the ATLAS Experiment - Detector, Trigger and Physics*, [arXiv:0901.0512 \[hep-ex\]](https://arxiv.org/abs/0901.0512).
- [12] ATLAS Collaboration, *Performance of the ATLAS Inner Detector Track and Vertex Reconstruction in the High Pile-Up LHC Environment*, Tech. Rep. ATLAS-CONF-2012-042, CERN, Geneva, Mar, 2012. <https://cds.cern.ch/record/1435196>.
- [13] R. Seuster, *Performance of the ATLAS Reconstruction Software with high level of Pileup in 2011*, *Journal of Physics: Conference Series* **396** (2012) no. 2, 022043.
- [14] G. F. Knoll, *Radiation detection and measurement*. Wiley, New York, 3rd ed., 2000.
- [15] M. Capeans, G. Darbo, K. Einsweiller, M. Elsing, T. Flick, M. Garcia-Sciveres, C. Gemme, H. Pernegger, O. Rohne, and R. Vuillermet, *ATLAS Insertable B-Layer Technical Design Report*, Tech. Rep. CERN-LHCC-2010-013. ATLAS-TDR-19, CERN, Geneva, Sep, 2010. <https://cds.cern.ch/record/1291633>.
- [16] F. Campabadal et al., *Design and performance of the ABCD3TA ASIC for readout of silicon strip detectors in the ATLAS semiconductor tracker*, *Nuclear Instruments and Methods in Physics Research Section A* **552** (2005) no. 3, 292 – 328.
- [17] ATLAS TRT Collaboration, *The ATLAS TRT Barrel Detector*, *Journal of Instrumentation* **3** (2008) no. 02, P02014.
- [18] ATLAS TRT Collaboration, *The ATLAS TRT electronics*, *Journal of Instrumentation* **3** (2008) no. 06, P06007.
- [19] ATLAS Collaboration, *TRT occupancy and tracking performance with large pileup*, Tech. Rep. ATL-COM-PHYS-2012-468, CERN, Geneva, May, 2012. <https://atlas.web.cern.ch/Atlas/GROUPS/PHYSICS/IDTRACKING/PublicPlots/ATL-COM-PHYS-2012-468/>.